Journal of Applied Physics

Evolution of planar defects during homoepitaxial growth of β-Ga_2O_3 layers on (100) substrates—A quantitative model

Cite as: J. Appl. Phys. **120**, 225308 (2016); https://doi.org/10.1063/1.4971957
Submitted: 02 November 2016 • Accepted: 24 November 2016 • Published Online: 15 December 2016

R. Schewski, M. Baldini, K. Irmscher, et al.

ARTICLES YOU MAY BE INTERESTED IN

A review of Ga_2O_3 materials, processing, and devices
Applied Physics Reviews **5**, 011301 (2018); https://doi.org/10.1063/1.5006941

Gallium oxide (Ga_2O_3) metal-semiconductor field-effect transistors on single-crystal β-Ga_2O_3 (010) substrates
Applied Physics Letters **100**, 013504 (2012); https://doi.org/10.1063/1.3674287

Step-flow growth in homoepitaxy of β-Ga_2O_3 (100)—The influence of the miscut direction and faceting
APL Materials **7**, 022515 (2019); https://doi.org/10.1063/1.5054943

Lock-in Amplifiers up to 600 MHz

© 2016 Author(s).

JOURNAL OF APPLIED PHYSICS **120**, 225308 (2016)

Evolution of planar defects during homoepitaxial growth of β-Ga_2O_3 layers on (100) substrates—A quantitative model

R. Schewski, M. Baldini, K. Irmscher, A. Fiedler, T. Markurt, B. Neuschulz, T. Remmele, T. Schulz, G. Wagner, Z. Galazka, and M. Albrecht
Leibniz-Institut für Kristallzüchtung, Max-Born-Straße 2, 12489 Berlin, Germany

(Received 2 November 2016; accepted 24 November 2016; published online 15 December 2016)

We study the homoepitaxial growth of β-Ga_2O_3 (100) grown by metal-organic vapour phase as dependent on miscut-angle vs. the *c* direction. Atomic force microscopy of layers grown on substrates with miscut-angles smaller than 2° reveals the growth proceeding through nucleation and growth of two-dimensional islands. With increasing miscut-angle, step meandering and finally step flow growth take place. While step-flow growth results in layers with high crystalline perfection, independent nucleation of two-dimensional islands causes double positioning on the (100) plane, resulting in twin lamellae and stacking mismatch boundaries. Applying nucleation theory in the mean field approach for vicinal surfaces, we can fit experimentally found values for the density of twin lamellae in epitaxial layers as dependent on the miscut-angle. The model yields a diffusion coefficient for Ga adatoms of $D = 7 \times 10^{-9}$ cm^2 s^{-1} at a growth temperature of 850 °C, two orders of magnitude lower than the values published for GaAs. © *2016 Author(s). All article content, except where otherwise noted, is licensed under a Creative Commons Attribution (CC BY) license (http://creativecommons.org/licenses/by/4.0/).* [http://dx.doi.org/10.1063/1.4971957]

I. INTRODUCTION

Monoclinic Ga_2O_3 (β-Ga_2O_3) is a semiconductor with a bandgap of 4.7 eV and an estimated break down field of 8 MVcm^{-1}.[1] It has recently attracted considerable interest as a promising material for applications such as solar blind UV photo detectors[2,3] and high power devices.[4,5] Epitaxial growth of structurally perfect crystalline layers with defined doping is a prerequisite to fully use its potential for device applications. In contrast to other wide bandgap semiconductors, large diameter substrates grown from the melt by methods like float zone,[6,7] edge defined film fed growth,[8] and Czochralski growth[9–11] are available. Homoepitaxial growth therefore is a natural choice. Homoepitaxial growth has been performed by molecular beam epitaxy,[1,12,13] halide vapor phase epitaxy,[14] and metal organic vapor phase epitaxy (MOVPE).[15,16] Though the (100) plane is the preferred cleavage plane of β-Ga_2O_3 and can be easily prepared, previous studies have shown that layers grown on substrates of this orientation suffer from a high density of twins and stacking faults.[15] These defects are harmful to electrical properties since they compensate the n-type doping, reduce the carrier mobility, and eventually lead to mobility collapse below a critical doping density.[17] In order to improve the materials structural perfection and to find proper growth conditions, the basic understanding of the formation mechanism of the planar defects is a prerequisite.

Formation of stacking faults and twin lamellae has been studied in early work on epitaxial growth of face centered cubic metals by Hall and Thompson,[18] and Dickson and Pashley.[19] Their models, later adopted for other material systems and crystal symmetries (e.g., SiC,[20] CdTe[21]), start from the assumption that growth on surface facets proceeds through nucleation and growth of two-dimensional islands. In case of a proper surface orientation, these islands have the choice to nucleate either in the epitaxial orientation or in the twinned orientation: In the latter case, they leave a coherent twin boundary behind at the interface between the island and the substrate. Formation of twin lamellae through double positioning is inhibited, if growth takes place in the step flow mode. This is promoted if at a given growth temperature the surface diffusion length of the adatoms is higher than the typical width of surface terraces, i.e. in this case adatoms will be able to reach the nearest step edge. Despite this qualitative understanding and pragmatic solutions, a quantitative model that describes twin lamella formation through double positioning has not been presented yet.

In this paper, we present detailed experimental results on twin lamella formation by double positioning in homoepitaxial growth of β-Ga_2O_3 on the (100) plane by MOVPE. We show that by appropriate choice of the miscut-angle and growth conditions, structurally perfect layers can be grown. Scanning transmission electron microscopy (STEM) reveals that the observed planar defects are twin lamellae that can be described by a *c*/2 glide reflection of the monoclinic lattice on the *a*-plane. Quantitative evaluation of the stacking fault densities from transmission electron microscopy (TEM) data shows a reduction of the stacking fault densities with increasing miscut-angle of the substrate. Applying nucleation theory in the mean field approximation[22,23] to fit the experimentally measured stacking fault densities vs. miscut-angle, we not only get excellent agreement to our experimental data but also obtain an experimentally measured diffusion constant *D* of the adatoms on the (100) surface for the growth of β-Ga_2O_3. At the growth temperature of 850 °C, we find a diffusion coefficient $D = 7 \times 10^{-9}$ cm^{2}s^{-1}, which is more than two orders of magnitude lower than that of Ga on GaAs[24] but 6 orders of magnitudes higher than in GaN.[25]

 © Author(s) 2016.

II. EXPERIMENTAL

Epitaxial layers are grown by metal organic vapor phase epitaxy onto semi-insulating (100) oriented β-Ga_2O_3 single crystals with a defined miscut-angles ranging from 0.1° up to 6° towards the c-orientation of the monoclinic lattice. Substrates are obtained from β-Ga_2O_3 single crystals, grown by the Czochralski method.[9] Residual surface damage after chemo-mechanical polishing is removed by annealing in oxygen atmosphere at 900 °C for 60 min, which results in surfaces that exhibit equidistant surface steps of about 0.59 nm height, corresponding to the distance between the (200) planes. Epitaxial layers are grown in a commercial vertical reactor from Structured Materials Industries (SMI) at a pressure of 5 mbar and a substrate temperature of 850 °C. Triethylgallium is used as a metalorganic Ga precursor. O_2 serves as an oxygen source. Further details on the growth can be found in Refs. 15 and 16.

From these epitaxial layers, we prepare cross-sectional TEM samples along the (010) orientation by plan parallel polishing to a thickness of about 10 μm. Final Ar^+ ion etching to electron transparency in a GATAN precision ion polishing system (PIPS) is performed using an acceleration voltage of 3.5 kV and an incident angle of 4° for Ar^+ ions. During thinning, the samples are cooled by liquid nitrogen to minimize residual irradiation damage. To remove residual surface damage generated by ion milling, we reduce the acceleration voltage stepwise to 0.2 kV while increasing the angle of the ion guns to 7°.

Transmission electron microscopy (TEM) and scanning transmission electron microscopy (STEM) are performed using an aberration corrected FEI Titan 80-300 microscope operated at 300 kV. The microscope is equipped with a Fischione high-angle annular dark-field detector (HAADF) and a highly brilliant field emission gun (X-FEG). The semi-convergence angle is tuned to 9° and the semi-acceptance angle of the detector is set to 35 mrad. In the case of β-Ga_2O_3 projected along the [010] direction, small thickness changes lead to strong changes in the high resolution transmission electron microscopic (HRTEM) lattice pattern, which makes the interpretation of the images rather difficult. Therefore, we focus on high-resolution mode STEM images which are more intuitive to interpret.

Atomic force microscopy (AFM) images were acquired by a Bruker Dimension Icon AFM in the tapping mode.

Structural models have been generated by the VESTA[26] 3D visualization software.

III. RESULTS

A. Surface morphology

Fig. 1 shows the atomic force microscopy images of the substrate surface with the surface normal tilted versus the [001] direction by miscut-angles α of 0.1°, 2°, 4°, and 6° along with those of the surface of epitaxial layers grown on them. All substrate surfaces prior to growth exhibit straight well aligned surface steps of half a unit cell height, independent of the respective miscut-angle. The as-grown surfaces of the sample with the lowest miscut-angle show the presence of three-dimensional islands. The islands elongate in the [010]-direction with a typical length of 200 nm and have a width of 100 nm in the [001]-direction. The aspect ratio of length to width (l/w) is 2, independent of the specific island length. For miscut-angles of 2°, the surface is still characterized by stepped three-dimensional islands. The steps have a typical height of half a

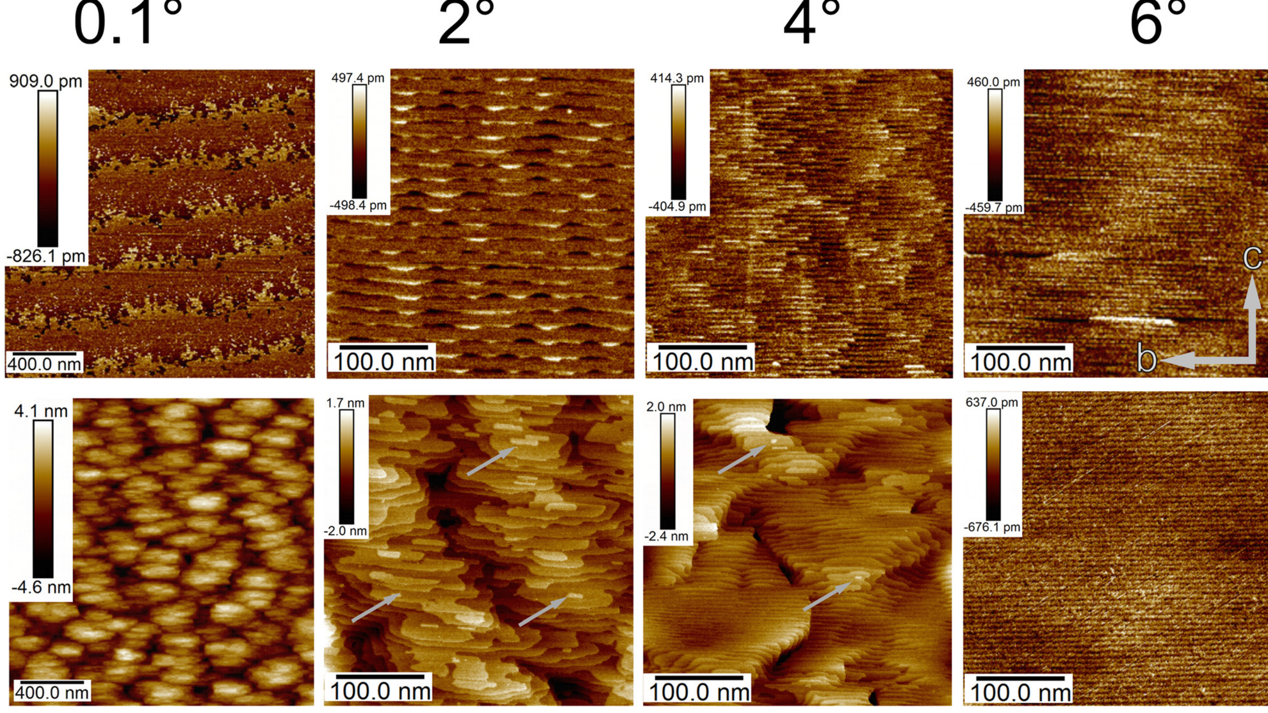

FIG. 1. AFM images of substrates with miscut-angles of 0.1°, 2°, 4°, and 6° towards *c* (upper row) and epitaxial grown layers on them (lower row). The substrate is characterized by equally spaced and regular arranged steps. The surface morphology undergoes a transition from 2D island growth to step-flow growth with increasing miscut-angle. The arrows indicate the presence of two-dimensional islands on the terraces.

unit cell along a. On the terraces, two-dimensional islands are visible (marked by arrows). For the sample with a miscut-angle of 4°, the overall surface morphology is characterized by extended surface steps along b and a terrace width of 6 nm. In areas where steps bunch and terraces with a width beyond 20 nm appear, two-dimensional islands are present. For a miscut-angle of 6° along the [001]-direction, regular steps aligned along b of half a unit cell height are observed and there is no apparent difference in the surface structure of substrate and the as grown epitaxial layers. Moreover, no signs of step bunching are visible despite the high miscut-angle. Summarizing the AFM results, we can state that layers with small miscut-angles $0 < \alpha < 2°$ vs. [001] are dominated by growth through nucleation and lateral growth of two-dimensional islands. Layers with a miscut-angle $\alpha \sim 6°$ vs. [001] are dominated by step flow growth.

B. Atomic structure of homoepitaxial layer

Fig. 2(a) shows a cross-sectional STEM-HAADF image of a layer grown on the substrate with a miscut-angle of 2°. The image shows the region close to the surface. Atomic column contrast arises from the gallium columns only. This is because the atomic number of oxygen ($Z = 8$) is essentially smaller than that of gallium ($Z = 31$) and Ga and oxygen atoms are too closely spaced. A number of steps are visible at the surface that have a height of half a unit cell along the surface normal. They have a spacing ranging between 10 and 20 nm, which corresponds considerably well to the expected value of 17 nm for the intended miscut-angle of 2°. Fig. 2(b) makes deviations in the stacking sequence visible in terms of a shift of the respective lattice plane with respect to a perfect crystal matrix (gradient of the geometrical phase; for details of the method, see Ref. 27). The grey background indicates the perfect lattice; dark/bright lines indicate areas where a phase shift is present in the structure. Two observations are of interest here. (i) In the region t1 at the top of the layer close to the surface, a periodic shift of the phase is visible. (ii) Deeper in the layer, we observe a line (marked by t2) that meanders through the whole layer alternating from (100) to (001)-planes and ends up at the surface. The underlying atomic structure of the defect marked t1 is shown in Fig. 2(c). It has a thickness of 1.75 unit cells along [100]. Its lower boundary in the (100) plane is indicated by the red

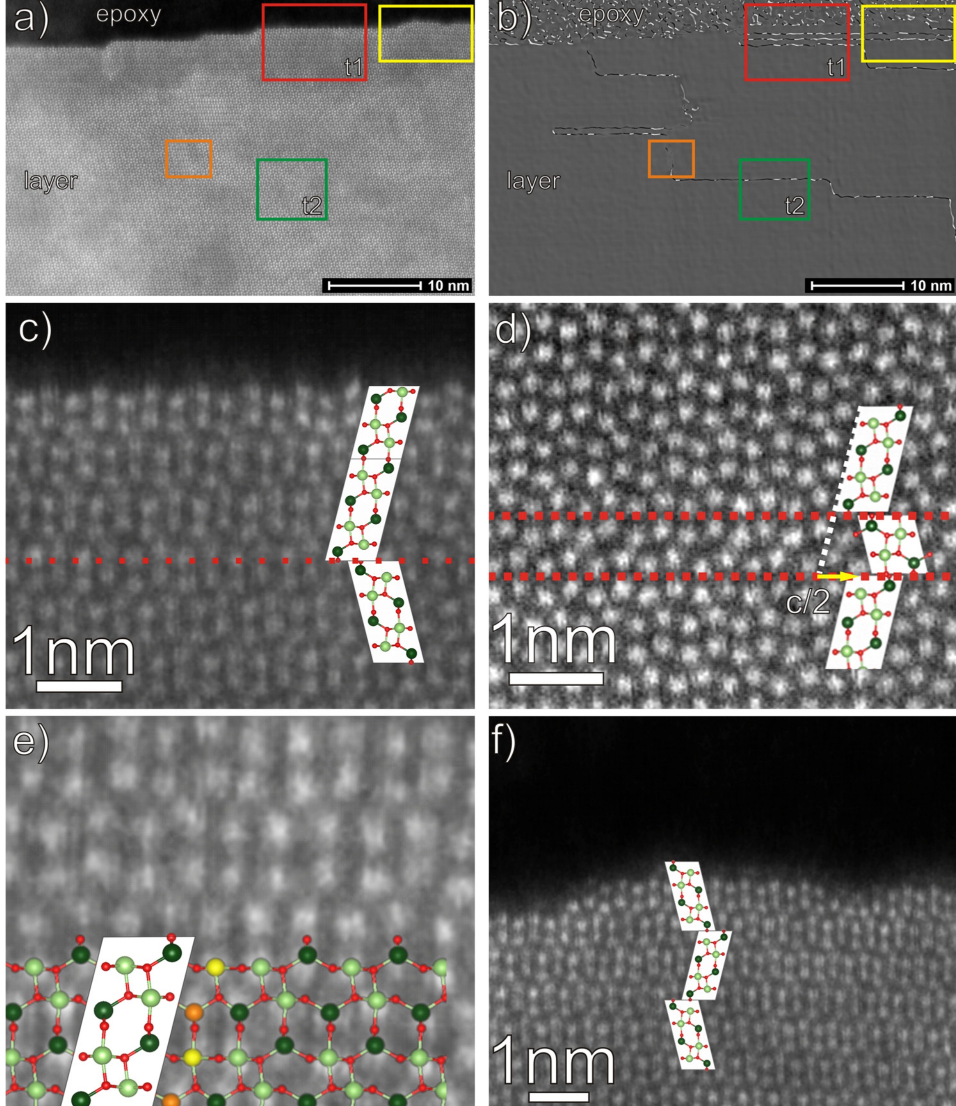

FIG. 2. Cross-sectional STEM HAADF images of an epitaxial layer grown on a substrate with a miscut-angle of 2°. The image is taken along the b-direction. Bright dots correspond to atomic Ga columns. Oxygen columns are not visible. The inset shows the unit cell in form of a stick and ball model. Defects are indicated by colored frames. (a) STEM HAADF overview of an area close to the surface. (b) Geometrical phase analysis of the micrograph shown in (a). Grey areas indicate the perfect lattice. Dark/bright lines indicate an error in the stacking sequence of the monoclinic lattice along a. (c) Enlarged detail of the twin t1 marked by a red square in Fig. (a). (d) Details of the defect t2 indicated by a green frame in (a). The defect is a twin lamella of half unit cell thickness. (e) Details of the defect indicated by orange frame in (a). The defect is a stacking mismatch boundary. It corresponds to an inserted c-plane. The plane is indicated by yellow and orange Ga atoms. (f) Twinned two-dimensional island coalescing with a surface step (indicated by a yellow frame in (a)).

dashed line. The upper boundary is the layer surface. At the lower boundary, it is obvious that the [001]-planes tilt. The relationship can be described crystallographically by a mirror operation at the (100) plane and a translation by a half ***c***-lattice parameter along the ***c*** direction. The defect t1 is a twin lamella of 1.75 unit cell thickness. For intuitiveness, the image has been overlaid with a stick and ball model of the lattice. The structural model shown in Fig. 2(c) reveals that all atoms in the boundary are fully coordinated, i.e., the (100) twin boundary is coherent.

An analysis of the atomic structure of the defect t2 is shown in Fig. 2(d). This defect is a twin lamella with a thickness of half a unit cell. It has two coherent boundaries at the upper and lower interfaces similar to those of the twin lamella t1. Because the layer has a thickness of half a unit cell, the matrix above the defect is shifted by half a c lattice parameter with respect to the surrounding matrix. This induces a stacking mismatch boundary lying on the (001)-plane. It essentially consists of an inserted half unit cell in the ***c*** direction. Fig. 2(e) shows a schematic of this boundary derived from the STEM image. In case this stacking mismatch boundary meets another half integer thick twin, the lattice symmetry is restored there but reproduced at the opposite site of twin and proceeds through the whole layer to the surface in a similar way. This climb is typical for twin lamella with a thickness of an odd number of half unit cells.

Let us now turn back to the surface. At the left hand side of Fig. 2(a), a two-dimensional island of half a unit cell thickness with a lateral extension of 4 nm coalesces with a surface step. Fig. 2(f) shows an enlarged image of this region. An intrusion between the island and the step is clearly visible. The island grows in a twinned crystal orientation with respect to the underlying lattice and the step with which it coalesces. Note that the height of half a unit cell and the lateral extension of 4 nm along the **b** direction correspond extremely well with that of the two-dimensional islands measured in the AFM images.

C. Evaluation of miscut-angle dependent density of twin lamella

Figs. 3(a)–3(d) show the typical TEM bright-field images of epitaxial layers grown on β-Ga_2O_3 (100) substrates with miscut-angles vs. [001] of 0.1°, 0.7°, 2°, and 4°, respectively. Twin lamellae are seen as dark lines lying on the (100) planes. Fig. 3(a) shows a micrograph of a layer grown on a substrate with the lowest miscut-angles. While the substrate is virtually free of twin lamella, the layer shows a high density of them homogeneously distributed throughout the layer. With increasing miscut-angle, the density of twin lamella reduces. For the layer with a miscut-angle of 4°, twin lamellae are visible only sporadically by TEM. Layers grown on substrates with a miscut-angle of 6° show no twin lamella at all within the field of view typical for TEM. For quantitative analysis, we count their number along the growth direction in bright field TEM images and divide it by the total layer thickness, the estimated layer depth in projection direction, and the image width. The density is measured in steps of 100 nm along the interface in every image. Samples have been typically investigated along the surface over a region of 100 μm in length. Table I displays the density of twin lamella as dependent on the miscut-angle and the respective nominal terrace width on the surface. The terrace width is calculated from the measured miscut-angle of the sample and the measured step height of $a/2$. The density of twins decreases with increasing miscut-angle. It reduces by more than two orders of magnitude when increasing the miscut-angle from 0.1° to 4°. At miscut-angles of around 6°, twin lamellae appear only occasionally and can be neglected. Table I summarizes the results of our measurements.

To estimate the growth rate, we performed growth runs with durations ranging from 1 to 60 min and measured the layer thickness from the site where twinning started. One may argue that for mainly 2D island nucleation and for step flow growth, one would expect different growth speeds. Our results, however, show that the growth speed is almost

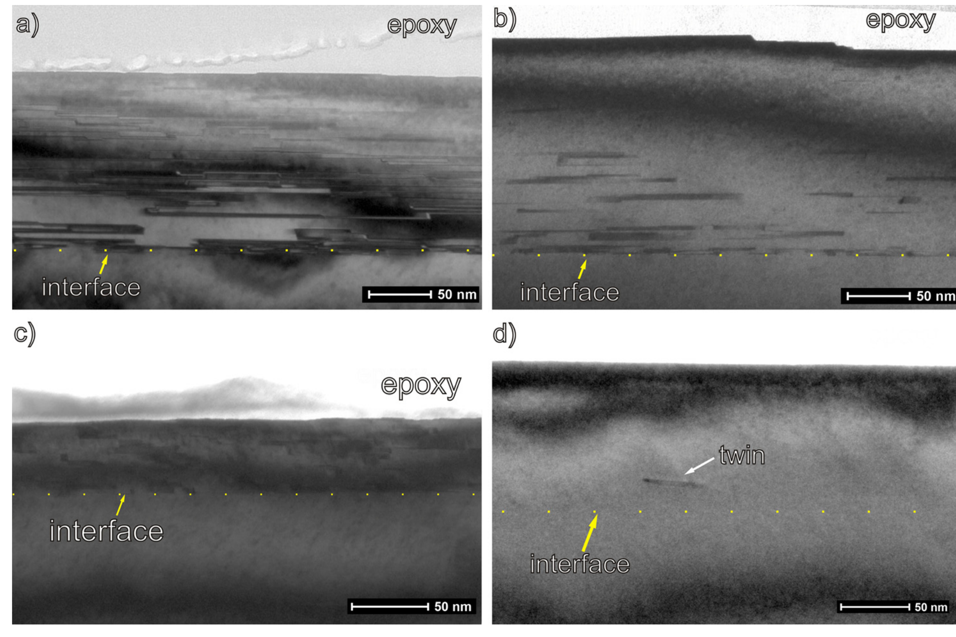

FIG. 3. TEM bright field images of layers grown on substrates with miscut-angle α of 0.1° (a), 0.7° (b), 2° (c), and 4° (d). Dark lines parallel to the surface are twin lamella.

TABLE I. Typical twin densities estimated from TEM in dependence of the substrate miscut-angle and the terrace width.

Miscut-angle [°]	Step length [nm]	Twin density [cm^{-3}]
0.1	340	1.0×10^{17}
0.3	110	9.2×10^{16}
0.7	50	5.2×10^{16}
1.4	25	4.7×10^{16}
4	8	5.5×10^{14}
6	5	~ 0

independent on the growth mode, and that the layer thickness increases linearly with growth time. From these series, we are able to estimate a growth speed of 0.04 monolayers per second (ML s^{-1}), where the thickness of one monolayer corresponds to half a unit cell in the *a* direction.

IV. DISCUSSION

A. Phenomenological description of twin formation

To discuss the origin and possible formation mechanism of the twin lamellae, we may summarize the main experimental observations.

(i) The surface morphology of homoepitaxial layers grown on (100) β-Ga_2O_3 substrates depends on the miscut-angle: For small miscut-angles ($0° < \alpha < 1°$), the surface morphology is characterized by three-dimensional islands. For intermediate miscut-angle ($1° < \alpha < 4°$), step-meandering and presence of two-dimensional islands are observed. At miscut-angles as high as 6°, perfect well-aligned steps are present, indicating step-flow growth.

(ii) Planar defects in the form of twin lamellae that can be described by a c/2 glide reflection of the monoclinic lattice are present in layers with low and intermediate miscut-angles.

(iii) The density of twin lamellae decreases with increasing miscut-angle of the substrate.

These experimental findings, especially the two-dimensional islands found in AFM and TEM images on the terraces and the decreasing density of twin lamella with increasing miscut-angle, strongly support double positioning as the mechanism that introduce twin lamella in our samples.

A schematic on twin formation by double positioning on Ga_2O_3 (100) facet is displayed in Fig. 4(a). Incoming adatoms attach to the (100) surface of Ga_2O_3 either in the epitaxial orientation or in the twinned orientation. Growth proceeds then laterally by attachment of further atoms and 2D island form, exhibiting either the epitaxial or the twinned orientation relationship, respectively. Although the epitaxial relation is energetically more favorable, the interface between the twinned 2D island and the substrate is fully coordinated in the epitaxial and in the twinned orientations. Incoherent lateral boundaries exhibiting dangling bonds form upon coalescence of a twinned and an epitaxial island. Once a closed layer has formed on the 2D islands, growth on top of them proceeds in a similar way. The probability of

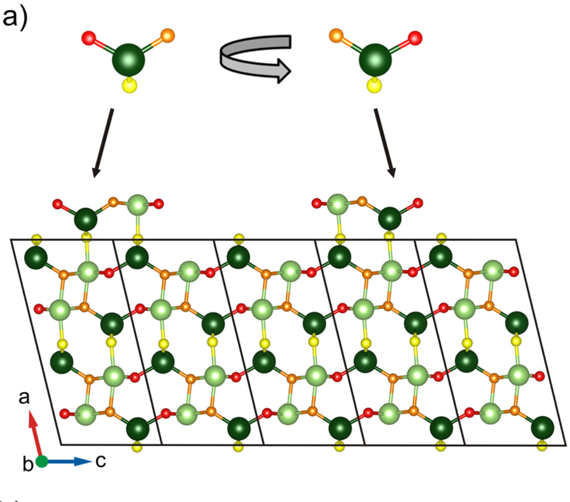

b)

surface diffusion > terrace width

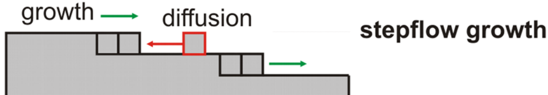

surface diffusion < terrace width

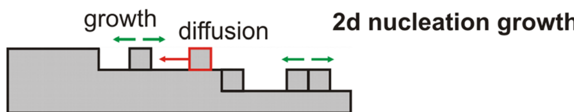

FIG. 4. (a) Stick and ball model illustrating the double positioning on the (100) plane of β-Ga_2O_3. Dark green and bright green balls correspond to tetrahedral (Ga I) and octahedral (Ga II) bound Gallium atoms, respectively. To enhance the visibility of the double positioning, the different oxygen sites OI, OII, and OIII have been colorized red, orange, and yellow, respectively. (b) Schematic sketch showing step-flow growth and growth proceeding through nucleation of two-dimensional islands.

islands to nucleate in a twinned orientation governs the resulting density of twin lamella in the film.

Real surfaces have finite miscut-angles and exhibit surface steps (Fig. 4(b)). Adatoms diffusion across the surface and the energetically preferred incorporation at step edges compete with 2D island nucleation. Growth at step edges is epitaxial. Through the competition with step edges, the probability to nucleate 2D islands on the terraces between the steps reduces. Whether 2D island growth or step–flow growth prevails essentially depends on the width of the terraces and the diffusion length of adatoms on the surface. For given growth conditions (temperature, flux of adatoms), the density of islands and thus of twins essentially depends on the miscut-angle.

B. A quantitative model on twin lamella formation on vicinal planes

In the following, we will present a quantitative model for twinning by double positioning. We adopt a model by Bales, originally developed to describe nucleation and growth of islands on a vicinal surface.[18,19] The basics of layer by layer

growth on step free surfaces through island nucleation have been described in an early work by Zinsmeister[28] and Frankl and Venables.[29] They describe nucleation of two-dimensional islands by a set of linear differential equations. These equations describe the development of the mean adatom density and island distribution with time, considering the incoming flux of adatoms and their diffusion on the growth surface. Later, Bales and Chrzan[22] could show that for a flat surface this model is in good agreement with Kinematic Monte Carlo (KMC) simulations. It has been later expanded by Bales[23] to describe the island densities on a vicinal substrate. Here, incoming adatoms are either incorporated into step edges or form two-dimensional islands.

Fig. 5 shows a schematic of the typical processes occurring during epitaxial growth on a stepped surface. Atoms impinge onto the perfect surface (a) with a flux F. Once adsorbed as adatoms, they diffuse with a diffusion constant D on the surface (b). They then attach to kink-sites at surface steps (c), meet other adatoms to form dimers (d), or attach to existing islands (either at island edges or on top of them) (f). Adatoms attached to islands or surface steps can detach or diffuse along the island edges or step edges, respectively. At high temperature, some adatoms can re-evaporate (e).

In the following, we will adopt the model by Bales for the nucleation on vicinal surfaces. Bales describes the time evolution of mean field quantities such as the mean density of adatoms $\langle n_1 \rangle$ and mean islands densities $\langle n_s \rangle$ for islands of consisting of s atoms, by a set of coupled ordinary differential equations. Either an adatom meets another adatom with a capture efficiency expressed as the capture number σ_1 or an island of size s with a capture number σ_s. Basic assumptions of the model are the following:

- The flux of atoms (monomers) to the surface is constant
- The surface consists of 2D islands and surface steps
- The 2D islands are uniformly distributed on the terrace between the step edges
- The supersaturation is high and there is no critical island size
- Polymers consisting of two or more adatoms are stable and may only grow in size but not dissociate
- There is no re-evaporation from the surface

In the framework of the mean field rate equation approach, the adatom density $\langle n_1 \rangle$ on a vicinal plane is then given by

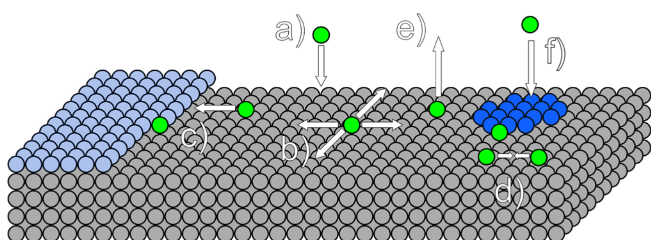

FIG. 5. Schematic sketch of the typical processes occurring during MOVPE growth: (a) Adsorption of adatoms on the substrate. (b) Diffusion of adatoms on the surface. (c) Incorporation of adatoms at a kink site of a surface step. (d) Nucleation of an island from encounter of two adatoms and incorporation of an adatom into an existing island. (e) Desorption of an adatom from the substrate. (f) Direct impingement of an adatom on an existing island.

$$\frac{1}{F}\frac{d\langle n_1\rangle}{dt} = \gamma - \frac{D}{F}\xi^{-2}\langle n_1\rangle - \frac{D}{F}\chi\langle n_1\rangle - k_1\langle n_1\rangle - \sum_{s=1}^{\infty} k_s\langle n_s\rangle, \tag{1}$$

with F being the flux of incoming atoms onto the growth surface (given in monolayer per second) and D the diffusion constant of the adatoms on the free surface. The generation rate γ of adatoms on the uncovered surface of atoms is given by $\gamma = \exp(-R \times t)$, with the arrival rate $R = F * b*c$ (b and c the lattice parameter).

The second term on the right hand side of Eq. (1) describes the loss of adatoms by attachment to a second adatom or attachment to an island formed of s adatoms, with ξ being the mean distance a monomer travels before colliding with an island or another adatom. It is given by

$$\xi^{-2} = 2\sigma_1\langle n_1\rangle + \sum_{s=2}^{\infty}\sigma_s\langle n_s\rangle. \tag{2}$$

The capture numbers σ_1 and σ_s are given by

$$\sigma_s = \frac{2\pi}{\gamma}\frac{\sqrt{s}}{\zeta}\frac{K_1(\sqrt{s}/\zeta)}{K_0(\sqrt{s}/\zeta)}, \tag{3}$$

where K_i is the modified Bessel function of the order i and ζ is the average distance a monomer travels before attaching to an island/adatom or a step

$$\zeta^{-2} = \xi^{-2} + \chi. \tag{4}$$

The third term of Eq. (1) corresponds to the loss of monomers to a step, where χ obeys to

$$\chi = \frac{\tanh\left(\frac{l}{2\xi}\right)}{\xi^2\left[\frac{l}{2\xi} - \tanh\left(\frac{l}{2\xi}\right)\right]}, \tag{5}$$

with l being the step width.

The two last terms of Eq. (1) account for the number of atoms deposited directly on the islands (process f), with $k_s = s^{2/d_f}$ with d_f the fractal dimension of the island (here $d_f = 2$).[30] Desorption of adatoms is neglected in these equations.

The density of stable islands of size s obeys the differential equation

$$\frac{1}{F}\frac{d\langle n_s\rangle}{dt} = \frac{D}{F}\sigma_{s-1}\langle n_1\rangle\langle n_{s-1}\rangle - \frac{D}{F}\sigma_s\langle n_1\rangle\langle n_s\rangle + k_{s-1}n_{s-1} - k_s\langle n_s\rangle \quad s = 2, 3, \ldots. \tag{6}$$

Here, the rate at which a particular island grows depends on the presence of the steps as well as of the mean density of the islands of size s.

The mean island size is obtained by solving the set of s coupled ordinary differential equations (1) and (6). Since we are interested in the absolute number of islands forming a layer, we have to integrate Equations (1) and (4) up to full

coverage. To do so, we need to solve self consistently the nonlinear equations (2)–(5) for each time step. The flux of incoming adatoms F and the diffusion constant D are free parameters, when fitting our experimentally observed densities of twin lamellae. In our simulations, we obtain the effective flux F onto the surface experimentally from the growth rate as measured by TEM and ellipsometry. Therefore, the diffusion constant D is the only remaining fitting parameter.

From our simulation, we find that the maximum of the island size distribution at full coverage can be located at $s \sim 900$. It is thus sufficient to set the maximal island size to 1500. The rate equation approach is usually only valid for small coverages. However, by comparing results of KMC simulations to those of the rate equation approach, Körner *et al.*[31] have shown that the latter approach fits kinetic simulations very well if islands are counted separately upon coalescence. In our case, twinned islands are easily distinguishable from the surrounding matrix even after coalescence, assuming that each twin lamella is generated from a single nucleation event.

Fig. 6 shows the fitted density of twin lamellae against the terrace width/miscut-angle for a flux of incoming atoms of 0.04 ML/s along with the experimentally observed density of twin lamellae that have a thickness of one monolayer (i.e., a thickness of half a unit cell in the ***a*** direction). For fitting, we assumed that the probability of nucleation in a twinned orientation is purely statistical, i.e., 0.5. The simulated curve fits the experimentally observed density of twin lamellae best for a diffusion constant $D = 7 \times 10^{-9}$ cm^2 s^{-1}. For low miscut-angles $<0.7°$, the density of twin lamella changes only very slightly, i.e., it corresponds to that on a perfect (100) facet and step edges have negligible influence on their density. In the transition region, i.e., for miscut-angles $0.7° < \alpha < 4°$, the density of stacking faults drops by two orders of magnitude. For high miscut-angles beyond 4°, the short terrace width promotes step-flow growth and the density of twin lamella is negligible. The excellent fit to our experimental data shows that formation of twin lamella occurs through double positioning and clearly arises from limited surface diffusion. In a recent paper,[32] we showed that on the (010) plane, it is the gallium flux that determines the

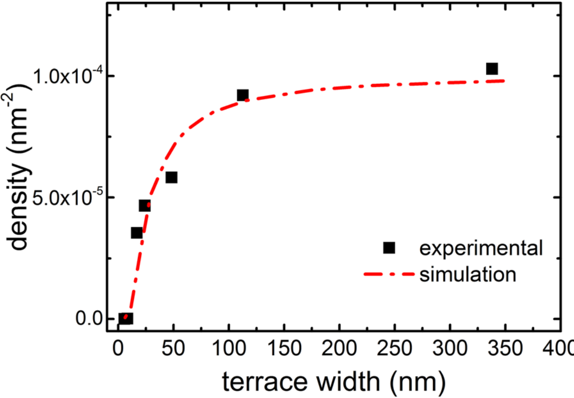

FIG. 6. Experimental nucleation densities per monolayer growth in dependence of the terrace width and the fitted curve to these experimental data for a diffusion constant of $D = 7 \times 10^{-9}$ cm^{-2} s^{-1}.

growth rate, while the influence of the oxygen flux can be neglected, i.e., growth is limited by Ga diffusion on the surface. We now may compare the obtained diffusion coefficient with published experimental data of other Ga based compounds such as GaAs or GaN. For GaAs, values ranging between 1.8×10^{-7}cm^{2}s^{-1} (Ref. 33) and 7×10^{-7} cm^{-2} (Ref. 24) (at our growth temperature of 850 °C) have been derived from the study of RHEED oscillations during MBE growth[34] and AFM measurements, respectively.[24] In case of GaN, only few experimental data have been published. Brandt *et al.* found a diffusion coefficient of 5×10^{-14} cm^2 s^{-1} for the case of cubic GaN from RHEED studies.[25] This low value is due to an essentially higher activation energy for surface diffusion (2.48 eV in the case of GaN)[25] than in GaAs (1.1 eV).[33] So surface diffusion on (100) β-Ga_2O_3 during MOVPE growth is two orders of magnitude lower than in GaAs but six orders of magnitude higher than in GaN. The latter holds at least for growth performed without surfactants. In fact, experiments performed with In as a surfactant have shown that it reduces the density of stacking faults by orders of magnitude.[35]

V. SUMMARY AND CONCLUSION

We have shown that homoepitaxial growth by MOVPE on (100) β-Ga_2O_3 is challenging since stacking faults in form of twin lamella are present in epitaxial layers. These defects are characterized by a $c/2$ glide reflection as twin relation. Coalescence of twinned and epitaxial 2D islands results in the formation of incoherent twin boundaries that exhibit dangling bonds leading to compensation and hamper the mobility of charge carriers.[17] Formation of these twin lamellae is a result of double positioning of 2D islands on the β-Ga_2O_3 (100) plane. Their density depends on miscut-angle and is a result of limited surface diffusion of the Ga-adatoms. Under the growth condition applied, we find step-flow growth and defect free material at miscut-angles $\alpha \sim 6°$. Adopting nucleation theory in the mean field approach, we are able to fit the experimentally observed stacking fault densities as dependent on the miscut-angle for the (100) surface. We achieve a value for the diffusion coefficient for surface diffusion of 7×10^{-9}cm^{-2} s^{-1} at the growth temperature of 850 °C. This value is two orders of magnitude lower than that experimentally found in GaAs but 6 orders of magnitude higher than values reported for cubic GaN. Preventing stacking fault formation requires promotion of surface diffusion by increased growth temperatures or application of surfactants that promote surface diffusion or reduction of terrace width by introducing substrates with high miscut-angles.

ACKNOWLEDGMENTS

This work was supported by Grant No. SAW-2012-IKZ-2 by the Leibniz-Gemeinschaft. We thank Konrad Tschernig and Nikolai Husung for the support in the implementation of the simulations. We thank Raimund Grünberg for performing AFM measurements.

[1]M. Higashiwaki, K. Sasaki, A. Kuramata, T. Masui, and S. Yamakoshi, Appl. Phys. Lett. **100**, 13504 (2012).

[2]R. Suzuki, S. Nakagomi, Y. Kokubun, N. Arai, and S. Ohira, Appl. Phys. Lett. **94**, 222102 (2009).
[3]W. S. Hwang, A. Verma, H. Peelaers, V. Protasenko, S. Rouvimov, H. (Grace) Xing, A. Seabaugh, W. Haensch, C. Van de Walle, Z. Galazka, M. Albrecht, R. Fornari, and D. Jena, Appl. Phys. Lett. **104**, 203111 (2014).
[4]M. Higashiwaki, K. Sasaki, A. Kuramata, T. Masui, and S. Yamakoshi, Phys. Status Solidi A **211**, 21 (2014).
[5]K. Sasaki, M. Higashiwaki, A. Kuramata, T. Masui, and S. Yamakoshi, J. Cryst. Growth **378**, 591 (2013).
[6]Y. Tomm, J. Ko, A. Yoshikawa, and T. Fukuda, Sol. Energy Mater. Sol. Cells **66**, 369 (2001).
[7]E. G. Villora, K. Shimamura, Y. Yoshikawa, K. Aoki, and N. Ichinose, J. Cryst. Growth **270**, 420 (2004).
[8]H. Aida, K. Nishiguchi, H. Takeda, N. Aota, K. Sunakawa, and Y. Yaguchi, Jpn. J. Appl. Phys. **47**, 8506 (2008).
[9]Z. Galazka, R. Uecker, K. Irmscher, M. Albrecht, D. Klimm, M. Pietsch, M. Brützam, R. Bertram, S. Ganschow, and R. Fornari, Cryst. Res. Technol. **45**, 1229 (2010).
[10]Z. Galazka, K. Irmscher, R. Uecker, R. Bertram, M. Pietsch, A. Kwasniewski, M. Naumann, T. Schulz, R. Schewski, D. Klimm, and M. Bickermann, J. Cryst. Growth **404**, 184 (2014).
[11]Z. Galazka, R. Uecker, D. Klimm, K. Irmscher, M. Naumann, M. Pietsch, A. Kwasniewski, R. Bertram, S. Ganschow, and M. Bickermann, ECS J. Solid State Sci. Technol. **6**, Q3007 (2017).
[12]K. Sasaki, A. Kuramata, T. Masui, E. G. Víllora, K. Shimamura, and S. Yamakoshi, Appl. Phys. Express **5**, 35502 (2012).
[13]M.-Y. Tsai, O. Bierwagen, M. E. White, and J. S. Speck, J. Vac. Sci. Technol., A **28**, 354 (2010).
[14]H. Murakami, K. Nomura, K. Goto, K. Sasaki, K. Kawara, Q. Tu Thieu, R. Togashi, Y. Kumagai, M. Higashiwaki, A. Kuramata, S. Yamakoshi, B. Monemar, A. Koukitu, Q. T. Thieu, R. Togashi, Y. Kumagai, M. Higashiwaki, A. Kuramata, S. Yamakoshi, B. Monemar, and A. Koukitu, Appl. Phys. Express **8**, 15503 (2015).
[15]G. Wagner, M. Baldini, D. Gogova, M. Schmidbauer, R. Schewski, M. Albrecht, Z. Galazka, D. Klimm, and R. Fornari, Phys. Status Solidi, A **211**, 27 (2014).
[16]M. Baldini, M. Albrecht, A. Fiedler, K. Irmscher, D. Klimm, R. Schewski, and G. Wagner, J. Mater. Sci. **51**, 3650 (2016).
[17]A. Fiedler, R. Schewski, M. Baldini, Z. Galazka, G. Wagner, M. Albrecht, and K. Irmscher, "Influence of incoherent twin boundaries on the electrical properties of β-Ga_2O_3 layers homoepitaxially grown by metal organic vapor phase epitaxy," (unpublished).
[18]M. J. Thompson and M. W. Hall, Br. J. Appl. Phys. **12**, 495 (1959), available at http://iopscience.iop.org/article/10.1088/0508-3443/12/9/312/meta.
[19]E. W. Dickson and P. W. Pashley, Philos. Mag. **7**, 1315 (1962).
[20]S. Roy, M. Portail, T. Chassagne, J. M. Chauveau, P. Vennéguès, and M. Zielinski, Appl. Phys. Lett. **95**, 81903 (2009).
[21]Y. Yan, M. M. Al-Jassim, and K. M. Jones, J. Appl. Phys. **94**, 2976 (2003).
[22]G. S. Bales and D. C. Chrzan, Phys. Rev. B **50**, 6057 (1994).
[23]G. S. Bales, Surf. Sci. **356**, L439 (1996).
[24]S. Bietti, C. Somaschini, L. Esposito, A. Fedorov, and S. Sanguinetti, J. Appl. Phys. **116**, 114311 (2014).
[25]O. Brandt, H. Yang, and K. H. Ploog, Phys. Rev. B **54**, 4432 (1996).
[26]K. Momma and F. Izumi, J. Appl. Crystallogr. **44**, 1272 (2011).
[27]M. J. Hytch, Scanning Microsc. **11**, 53 (1997), available at http://www.ecmjournal.org/journal/smi/pdf/smi97-05.pdf.
[28]G. Zinsmeister, Vacuum **16**, 529 (1965).
[29]D. Frankl and J. Venables, Adv. Phys. **19**, 409 (1970).
[30]M. N. Popescu, J. G. Amar, and F. Family, Phys. Rev. Lett. **86**, 3092 (2001).
[31]M. Körner, M. Einax, and P. Maass, Phys. Rev. B **86**, 085403 (2012).
[32]M. Baldini, M. Albrecht, A. Fiedler, K. Irmscher, R. Schewski, and G. Wagner, ECS J. Solid State Sci. Technol. **6**, Q3040 (2017).
[33]T. Nishinaga and K. I. Cho, Jpn. J. Appl. Phys. **27**, L12 (1988).
[34]J. H. Neave, P. J. Dobson, B. A. Joyce, and J. Zhang, Appl. Phys. Lett. **47**, 100 (1985).
[35]M. Baldini, M. Albrecht, D. Gogova, R. Schewski, and G. Wagner, Semicond. Sci. Technol. **30**, 024013 (2015).